Microporous and Mesoporous Materials 170 (2013) 266–273

Contents lists available at SciVerse ScienceDirect

Microporous and Mesoporous Materials

journal homepage: www.elsevier.com/locate/micromeso

# Facile and surfactant-free route to mesoporous silica-based adsorbents from TFT-LCD industrial waste powder for $CO_2$ capture

Liang-Yi Lin, Hsunling Bai *

*Institute of Environmental Engineering, National Chiao Tung University, Hsinchu 300, Taiwan*

ARTICLE INFO

*Article history:*
Received 9 October 2012
Received in revised form 19 November 2012
Accepted 11 December 2012
Available online 20 December 2012

*Keywords:*
Surfactant-free
Mesoporous silica
TFT-LCD waste powder
$CO_2$ adsorption

ABSTRACT

A surfactant-free preparation of mesoporous silica spherical particles, MSPs was developed using sodium silicate extracted from TFT-LCD industrial waste powder via aerosol spray route in this study. Inorganic acids including hydrochloric acids and nitric acids were employed to acidify the silicate supernatant to form activated silica precursors and the influence of acids in the activated silica precursors was studied. The MSPs($HNO_3$), which was synthesized in the presence of nitric acids exhibited high surface area (776 $m^2/g$), mesopore size (5.3 nm) as well as large pore volume (1.15 $cm^3/g$) and it was further applied as a support of adsorbent for $CO_2$ capture. It was demonstrated that tetraethylenepentamine (TEPA)-impregnated MSPs($HNO_3$) adsorbent presents advantages of convenient synthesis, low cost and high adsorption performance (122 mg-$CO_2$/g-adsorbent), which was superior to those of TEPA-SBA-15 and TEPA-MCM-41 manufactured from pure silica chemicals under the same test conditions. The results suggested that low-cost MSPs($HNO_3$) prepared using silicate solution from TFT-LCD waste powder via spray approach can be promising $CO_2$ adsorbents. This novel process could also be employed for further extensible to other kinds of Si-related industrial wastes and benefit in large-scale production of highly valuable silica-based sorbents for environmental protection applications.



## 1. Introduction

The carbon dioxide ($CO_2$) capture and storage (CCS) technologies have received out-breaking concerns after the Kyoto Protocol came into force in 2005 [1]. Among capturing technologies, amine-supported mesoporous silicas for $CO_2$ adsorption are of particular interest because of their efficient adsorption performance, rapid mass transfer kinetics and simplicity of cyclic regeneration under mild conditions [2]. Several studies have shown that these aminated mesoporous silica adsorbents are useful for practical applications, such as those relevant in flue gas and for capture $CO_2$ from ambient air [3–5]. To this end, various mesoporous silicas including MCM-41 [6], SBA-15 [7], HMS [8] and KIT [9], etc. have been widely investigated on $CO_2$ adsorption in terms of adsorption capacity, regeneration ability and tolerance under water-existing environment.

Even though each family of mesoporous silica has its advantages; most of them were manufactured through solution precipitation methods using batch reactors, which require multi-step and time-consuming procedures. For example, the MCM-41 material is one of the mesoporous products made by the hydrothermal method which commonly proceeds at 100–150 °C for tens of hours [10]. An alternative approach to mesoporous silicas is the exploitation of vapor-phase routes which is the continuous flow set-up and this allows an easy scale-up of the synthesis [11–14]. Mesoporous silica spherical particles (MSPs), which were synthesized over aerosol-assisted continuous process, are relatively novel materials for environmental protection applications [15]. The spherical MSPs presents advantages of higher production rate, higher packing density and lower pressure drop than those mesoporous materials manufactured via batch processes. These advantages make MSPs more practical for gas adsorption and separation in terms of overall engineering considerations.

Very recently, Wang et al. [16] employed the amine-impregnated MSPs as adsorbents for $CO_2$ capture from flue gas streams. The results clearly demonstrated that the aminated MSPs can be considered as efficient and stable adsorbents in the prolonged cyclic $CO_2$ adsorption tests. However, they may pose problems in practical field applications because of their relatively high manufacturing costs and this would be one of the most important considerations for industrial applications. The high costs of MSPs are mainly due to the use of expensive surfactants as mesostructure-directing templates, which constitute almost 80% of total manufacturing costs. Furthermore, a subsequent thermal treatment is also required to remove the organic surfactants from the silica/surfactant hybrids,

* Corresponding author. Address: Institute of Environmental Engineering, National Chiao Tung University, 1001 University Rd., Hsinchu 300, Taiwan. Tel.: +886 3 5731868; fax: +886 3 5725958.
*E-mail address:* hlbai@mail.nctu.edu.tw (H. Bai).

1387-1811/$ - see front matter © 2012 Elsevier Inc. All rights reserved.
http://dx.doi.org/10.1016/j.micromeso.2012.12.019

which would further increase the energy penalty and costs. Thus the industrial applications of current methods would have certain limitations. Taking into account the potential scale involved in the production of MSPs for $CO_2$ capture, it is preferable to employ low-cost and abundant resources as precursors.

In this work, motivated by the aforementioned situation, the aerosol synthesis of low-cost MSPs was developed by employing sodium silicate solution as the silica source without adding extra surfactants. The sodium silicate solution, which is extracted from industrial waste powder of thin film transistor-liquid crystal display (TFT-LCD) industry, has been proven to be a feasible resource for preparing silica-based materials in our prior study [17]. The structural properties, morphology and formation mechanism of the prepared MSPs are presented and discussed. In addition, the cost-effectiveness of the obtained MSPs in terms of $CO_2$ adsorption is evaluated and compared to those of MCM-41 and SBA-15 samples prepared from TFT-LCD waste powder as well.

## 2. Experimental section

### 2.1. Aerosol fabrication of MSPs from waste-derived sodium silicate

Fig. 1 depicts the experimental setup of the reactor for continuously synthesizing the MSPs via ultrasonic spray process. The sodium silicate solution was prepared by mixing TFT-LCD waste powder with 6 M NaOH solution at room temperature for 3 h. Table 1 shows the elemental analysis of the raw waste powder and the silicate solution after extraction with NaOH solution. The sodium silicate solution was then acidified by adding hydrochloric acid or nitric acid, and the molar composition of the precursor mixture was $1SiO_2$:$359H_2O$:8HCl and $1SiO_2$:$359H_2O$:$3.7HNO_3$, respectively. The solution was then nebulized by an ultrasonic atomizer (1.8 MHz) with a dry and clean air stream of 2 slpm flow rate and the droplets were passed through a heating zone in which the temperature was controlled at 400 °C. The total reaction time of this continuous flow process was approximately 4 s. After the heating process, the as-synthesized MSPs samples were collected downstream of the reactor by a high-efficiency filter. Finally, they were recovered by washing and filtration with DI water followed by drying in an oven at 110 °C. The aerosol processing of MSPs samples from the waste-derived silicate in the presence of hydrochloric acid was denoted as MSPs(HCl), while the MSPs sample from the waste-derived silicate with the aid of nitric acid was named as MSPs($HNO_3$).

### 2.2. Hydrothermal synthesis of MCM-41 and SBA-15 from waste-derived silicate

The synthesis of recycled MCM-41 was performed using waste-derived silicate solution and cetyltrimethylammonium bromide (CTAB) as the silica source and template, respectively. The molar composition of the gel mixture was $1SiO_2$:0.2CTAB:$120H_2O$:$0.89H_2SO_4$. In a typical procedure, 89 ml of waste silicate solution was firstly acidified by adding approximately 40 ml of 4 N $H_2SO_4$ to bring down the pH to 10.5 with constant stirring to form a gel. After stirring, 7.28 g of CTAB (dissolved in 25 ml of DI water) was added drop by drop into the above mixture and the combined mixture was stirred for three additional hours. The resulting gel mixture was transferred into a Teflon coated autoclave and kept in an oven at 145 °C for 36 h. After cooling to room temperature, the resultant solid was recovered by filtration, washed with DI water and dried in an oven at 110 °C for 8 h. Finally, the organic template was removed by using a muffle furnace in air at 550 °C for 6 h.

**Table 1**
Elemental analysis of raw waste powder and silicate supernatant analyzed by the SEM-EDS and ICP-MS.

| Element | Si | F | O | N | Na |
|---|---|---|---|---|---|
| Raw waste powder (wt.%)[a] | 28.82 | 47.82 | 17.54 | 5.82 | – |
| Supernatant (ppm)[b] | 32750 | – | –[c] | – | 84220 |

[a] Sample analyzed by the SEM-EDS analysis.
[b] Sample analyzed by the ICP-MS analysis.
[c] Non-detected.

Recycled SBA-15 was synthesized using a tri-block copolymer, $EO_{20}$-$PO_{70}$-$EO_{20}$ (Pluronic P123, BASF) as the template and waste silicate solution as the silica source. The molar composition of the gel mixture was $1SiO_2$:0.02 P123:$286H_2O$:$4.2H_2SO_4$. For a typical synthesis, 2.01 g of P123 was dissolved in 20 g of DI water; meanwhile, 82 ml of waste silicate solution was added to 70 ml of 1 M $H_2SO_4$ to achieve the pH value of 2. Subsequently, calculated amounts of 6 M NaOH were added to the above silicate mixture to bring up the pH to 5 to accelerate the hydrolytic condensation reaction. After stirring, the surfactant solution was added slowly into the above mixture and the combined mixture was stirred for 15 min. The resulting gel mixture was transferred into a Teflon coated autoclave and kept in an oven at 100 °C for 24 h. After cooling to room temperature, the resultant solid was recovered by filtration, washed with DI water and dried in an oven at 60 °C for 24 h. Finally, the organic template was removed by using a muffle furnace in air at 500 °C for 6 h. The recycled MCM-41 and SBA-15 materials using waste-derived-silicate solution as silica source was denoted as R-MCM-41 and R-SBA-15, respectively.

For comparison purpose, the preparation of MCM-41 and SBA-15 from commercial silicate precursors was presented as well. The synthesis of MCM-41 was carried out using pure chemicals of sodium metasilicate nanohydrate ($Na_2SiO_3{\cdot}9H_2O$) following similar procedures described previously in the synthesis of R-MCM-41. The molar composition of the gel mixture was $1SiO_2$:0.2-CTAB:$120H_2O$:$0.89H_2SO_4$. Mesoporous SBA-15 was synthesized using a tri-block copolymer, $EO_{20}$-$PO_{70}$-$EO_{20}$ (Pluronic P123, BASF) as the template and sodium silicate solution (~14% NaOH, ~27% $SiO_2$, Aldrich) as the silica source, with similar procedures described in the synthesis of R-SBA-15. The molar composition of the gel mixture was $1SiO_2$:0.01P123:$286H_2O$:$0.7H_2SO_4$.

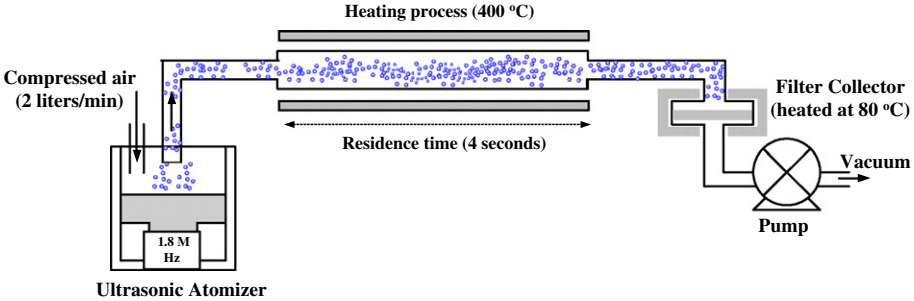


**Fig. 1.** Experimental setup for the fabrication of MSPs through ultrasonic spray process.

### 2.3. Characterization

The elemental analysis of the raw waste powder was determined by energy-dispersive X-ray spectroscopy in a scanning electron microscope (SEM-EDS, HITACHI-S4700). And the silicate supernatant was also analyzed by ICP-MS (SCIEX ELAN 5000- Inductively Coupled Plasma-Mass Spectrometer). Powder low angle X-ray diffraction patterns of prepared samples were recorded by using Rigaku X-ray diffractometer equipped with nickel-filtered CuKα ($\lambda$ = 1.5405 Å) radiation. The diffractograms of the mesoporous samples were recorded in the 2$\theta$ range 5–80° in steps of 0.6° with a count time of 60 s at each point. The specific surface area, specific pore volume and average pore diameter (BJH method) of the samples were measured by $N_2$ adsorption–desorption isotherms at 77 K using a surface area analyzer (Micromeritics, ASAP 2000). All the samples were degassed for 6 h at 350 °C under vacuum ($10^{-6}$ mbar) prior to the adsorption experiments. The morphology of the materials was observed via the SEM (HITACHI-S4700) images. TEM images of the samples were observed with a JEOL JEM 1210 TEM instrument operated at 120 keV and the samples (5–10 mg) were ultrasonicated in ethanol and dispersed on carbon film supported on copper grids (200 mesh).

### 2.4. $CO_2$ adsorption measurement

Mesoporous supports including MSPs(HCl), MSPs($HNO_3$), R-MCM-41, R-SBA-15, MCM-41 and SBA-15 were functionalized with tetraethylenepentamine (TEPA) at a weight ratio of 1:1 by the wet impregnation method reported by Lin et al. [17]. The $CO_2$ adsorption tests were conducted by a thermo-gravimetric analyzer (TGA, Netzsch TG209 F1, Germany). Typically, approximately 10 mg of adsorbents were loaded on the TGA sample holder and purged with nitrogen gas at the temperature of 110 °C with a flow rate of 120 $cm^3$/min for 30 min until the weight is not changed, which implies that the evaporation of water on the adsorbents was complete. The mass change of the adsorbents during $CO_2$ adsorption was then recorded under isothermal condition of 60 °C. The inlet $CO_2$ concentration was 15% (v/v in $N_2$) which was obtained from a certified gas cylinder and introduced at a flow rate of 40 $cm^3$/min (25 °C, 1 atm) for 60 min of adsorption time until the weight was not changed to ensure that the adsorbents were completely saturated. The moisture in the $CO_2$ gas cylinder was measured to be 5% relative humidity, which corresponded to an absolute moisture content of only 0.16% (v/v). This was much lower than the $CO_2$ concentration and thus the moisture impact on the $CO_2$ adsorption is negligible.

## 3. Results and discussion

### 3.1. Characterization of MSPs

Fig. 2 shows the powder XRD patterns of the as-prepared and washed MSPs samples, which were synthesized using sodium silicate supernatant from TFT-LCD waste powder through ultrasonic spray process. It can be seen that the as-prepared MSPs($HNO_3$) sample shows significant diffraction peaks at 2$\theta$ of 23°, 29°, 32°, 35°, 39°, 42°, 48° and 56°, which are indexed on $NaNO_3$ crystallites [18]. On the other hand, strong diffraction peaks located at 2$\theta$ of 27°, 32°, 45°, 56°, 66° and 75° of crystalline NaCl [19] were identified in as-prepared MSPs(HCl) sample. To elucidate the above findings, the general theory of acidification of sodium silicate must be addressed. In the preparation of activated silica precursors, sodium silicate was acidified and the silica condensation reactions would take place simultaneously to form a siloxane linkage between surface silanol groups, which can be represented as [20]:

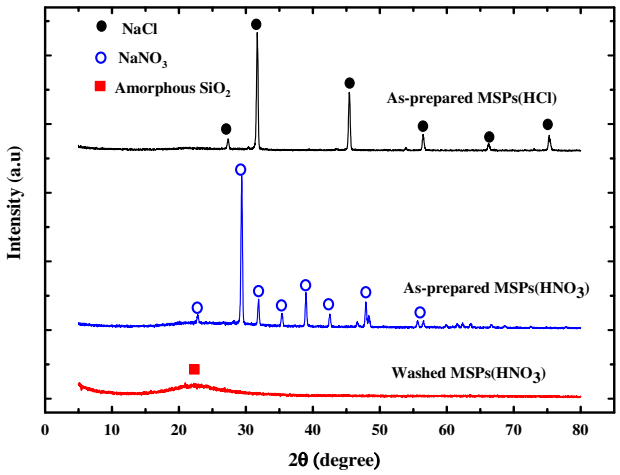


**Fig. 2.** XRD pattern of as-prepared MSPs(HCl), as-prepared MSPs($HNO_3$) and washed MSPs($HNO_3$) samples.

$$Si(OH)_4 + HO{-}Si(OH)_3 \rightarrow (OH)_3Si{-}O{-}Si(OH)_3 + H_2O \quad (1)$$

And the reaction of sodium silicate solution acidified with hydrochloric acid and nitric acid, respectively, during acidification process can be expressed as:

$$Na_2O \cdot xSiO_2 + 2HNO_3 \rightarrow xSiO_2 \downarrow + 2NaNO_3 + H_2O \quad (2)$$

$$Na_2O \cdot xSiO_2 + 2HCl \rightarrow xSiO_2 \downarrow + 2NaCl + H_2O \quad (3)$$

As the sodium silicate supernatant is acidified by nitric acid or hydrochloric acid, fine crystalline components of $NaNO_3$ or NaCl are formed. They were further solidified and embedded in silica spheres during spray and heating processes. Since $NaNO_3$ and NaCl exhibit stronger crystallinity than that of amorphous silica, the sodium salt crystallites are expected to show higher diffraction intensity as depicted in Fig. 2. Besides, these sodium salts are highly soluble so that they can be easily removed by water washing, leading to form pure siliceous MSPs materials. This is confirmed by XRD results in which a broad diffraction peak at 2$\theta$ of 22° of amorphous silica [21] is observed in the washed MSPs($HNO_3$) sample.

The thermal behavior of the MSPs samples was subsequently investigated using TGA and DTG analyses as shown in Fig. 3(a) and (b), respectively. One can see from Fig. 3(a) that both as-prepared MSPs(HCl) and MSPs($HNO_3$) samples show initial weight losses from 100 to 400 °C, which can be ascribed to the evaporation of the physically and chemically adsorbed water on the surface of the material. Furthermore, it is noticeable that there is a drastic weight losses from 600 to 800 °C of as-prepared MSPs($HNO_3$) as depicted in Fig. 3(b), and this is probably due to the thermal decomposition of crystalline $NaNO_3$ [19]. In the present study, the aerosol processing of MSPs(HCl) or MSPs($HNO_3$) samples was carried out at 400 °C in which the occluded NaCl or $NaNO_3$ salt can retain thermally stable. After aqueous washing, the washed MSPs($HNO_3$) presented high thermal stability up to 900 °C, and this clearly reveals that aqueous washing is an effective process to remove the sodium salts from the as-prepared MSPs materials. This is in agreement with the XRD result which confirms the presence of pure siliceous material of the washed MSPs.

Fig. 4(a) shows the $N_2$ physisorption isotherms of raw waste powder and washed MSPs materials. It is clear that raw waste powder exhibits a typical type II isotherm of non-porous materials according to the IUPAC classification. On the other hand, all washed MSPs samples show type IV isotherms with a well-defined capillary step, which are indicative of mesoporous materials [22]. The MSPs(HCl) sample shows the H3-type hysteresis loop, which

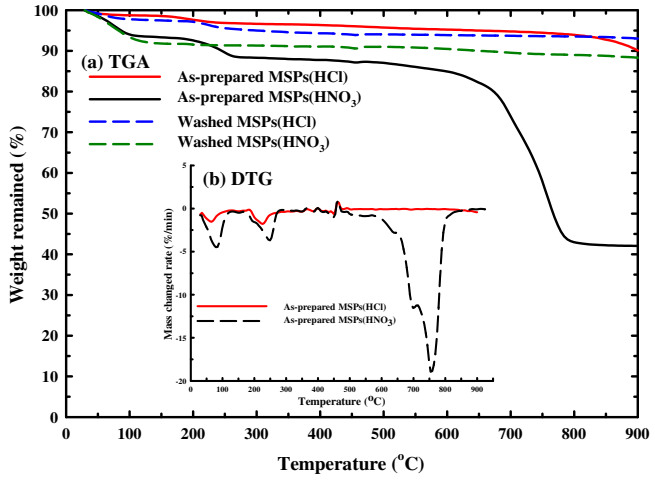


**Fig. 3.** (a) TGA and (b) DTG analyses of as-prepared and washed MSPs materials.

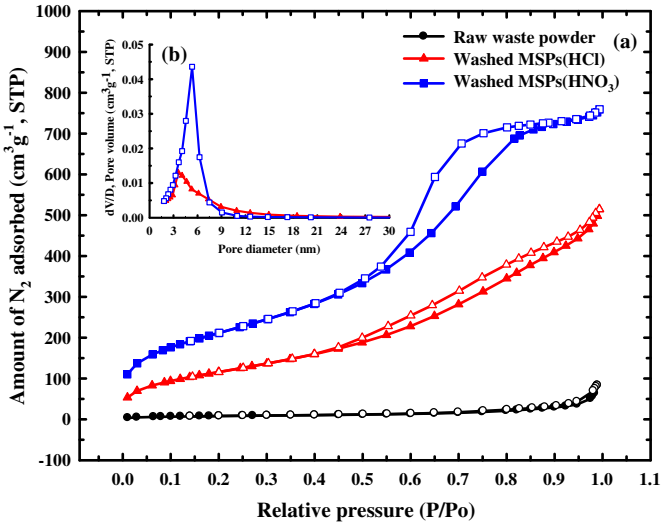


**Fig. 4.** (a) $N_2$ adsorption–desorption isotherms of raw waste powder, washed MSPs(HCl) and washed MSPs($HNO_3$) samples; (b) corresponding BJH pore size distribution of washed MSPs(HCl) and MSPs($HNO_3$) samples.

is assigned to the mesoporous system with slit-like shapes [23]. In contrast, the washed MSPs($HNO_3$) shows significantly higher adsorption capacity. It is noticeable that the sorption isotherm of washed MSPs($HNO_3$) sample has H2-like hysteresis loop, which is remarkably different from the washed MSPs(HCl). The H2-like hysteresis loop is typically attributed to the presence of ink-bottle-like mesopores. Besides, the hysteresis loop of MSPs($HNO_3$) tends to shift toward higher values of relative pressure as compared to MSPs(HCl), which implies that MSPs($HNO_3$) exhibits larger pore diameter. This result is further confirmed by the BJH pore size distribution shown in Fig. 4(b), where MSPs($HNO_3$) possesses narrow pore size distribution with a peak centered at 5.3 nm, larger than that of MSPs(HCl) with pore diameter located at 3.6 nm.

The template effect from the inorganic salts on the physical properties including BET specific surface area, total pore volume and BJH pore diameter derived from $N_2$ physisorption measurement are summarized in Table 2. It is seen that the as-prepared MSPs materials show low specific surface area and no porosities; however, the surface area and porosities of the washed MSPs materials are significantly enhanced after the removal of salt templates by aqueous washing process. This clearly implies that both sodium salts of NaCl and $NaNO_3$, which are formed during the sodium silicate acidification process, can be employed as effective templates to support the mesostructure. Moreover, washed MSPs($HNO_3$) shows higher specific surface area and larger pores as compared to MSPs(HCl) sample. These results are quite conclusive in demonstrating that the difference in the features of the pore geometry seems to be correlated to different occluded salt templates.

SEM image of the washed MSPs($HNO_3$) samples, as depicted in Fig. 5(a), shows that there are spherical particles with porous surface. On the contrary, the MSPs(HCl) sample mainly consists of crushed and fractured particles (Fig. 5(b)). TEM image in Fig. 5(c) further proves that the washed MSPs($HNO_3$) particles are porous, appears to consist of interconnected network, whereas the washed MSPs(HCl) shows hollow and crushed structures (Fig. 5(d)). Moreover, the chemical composition of the washed MSPs($HNO_3$) was analyzed by EDX analysis (Fig. 5(e)), where there are only Si and O elements observed (Cu peak from the TEM grid). This is in line with the XRD result, which confirms the presence of amorphous silica. Consequently, it can conclude from the results of XRD, $N_2$ physisorption measurement and EDX spectrum that silica spherical particles with open mesoporous structure can be prepared using sodium silicate solution extracted from TFT-LCD industrial waste powder as the silica precursor via surfactant-free aerosol route.

The schematic representation for the formation mechanism of MSPs(HCl) and MSPs($HNO_3$) samples through aerosol process is shown in Fig. 6. In this work, activated silica sols were firstly prepared by acidifying the sodium silicate supernatant extracted from TFT-LCD industrial waste powder with the aid of hydrochloric acid or nitric acid. Meanwhile, the sodium salt of NaCl or $NaNO_3$ crystallite is formed during acidification process. When the precursor solution is aerosolized and heated at 400 °C, the rapid evaporation of water drastically enhanced the silica polymerization and resulted in an increased concentration of salts simultaneously. As this process continues, these salts would precipitate out of the droplet at the air interface, forming a crust where the concentration is the highest. As water evaporation occurs at 400 °C, the occluded $NaNO_3$ salt with melting point of 308 °C in as-prepared MSPs($HNO_3$) would become molten and serves as a solvent, diffusing back into the core in response to the concentration gradient. Finally, the MSPs($HNO_3$) with interconnected mesoporous framework are produced after the removal of salts by water washing. In contrast, fractured particles were observed in washed MSPs(HCl). During the process, the solid shell of NaCl is formed in the beginning where the concentration is the highest. When the water evaporation occurs at 400 °C, the

**Table 2**
Physical properties of mesoporous silica-based adsorbents.

| Sample name | $S_{BET}$[a] ($m^2$/g) | $d_{BJH}$[b] (nm) | $V_p$[c] ($cm^3$/g) |
|---|---|---|---|
| Raw waste powder | 30 | – | 0.07 |
| As-prepared MSPs(HCl) | 16 | – | 0.05 |
| As-prepared MSPs($HNO_3$) | 19 | – | 0.08 |
| Washed MSPs(HCl) | 434 | 3.6 | 0.72 |
| Washed MSPs($HNO_3$) | 776 | 5.3 | 1.15 |
| MCM-41 | 1101 | 3.1 | 1.00 |
| SBA-15 | 745 | 6.5 | 1.02 |
| R-MCM-41 | 1083 | 3.0 | 0.99 |
| R-SBA-15 | 661 | 9.1 | 1.50 |
| TEPA-MSPs(HCl) | 2.5 | – | 0.001 |
| TEPA-MSPs($HNO_3$) | 51 | 5.0 | 0.13 |
| TEPA-MCM-41 | 53 | – | 0.15 |
| TEPA-SBA-15 | 40 | 5.0 | 0.11 |
| TEPA-R-MCM-41 | 55 | – | 0.14 |
| TEPA-R-SBA-15 | 30 | 8.7 | 0.48 |

[a] ET surface area.
[b] Pore diameter calculated by BJH theory.
[c] Total pore volume.

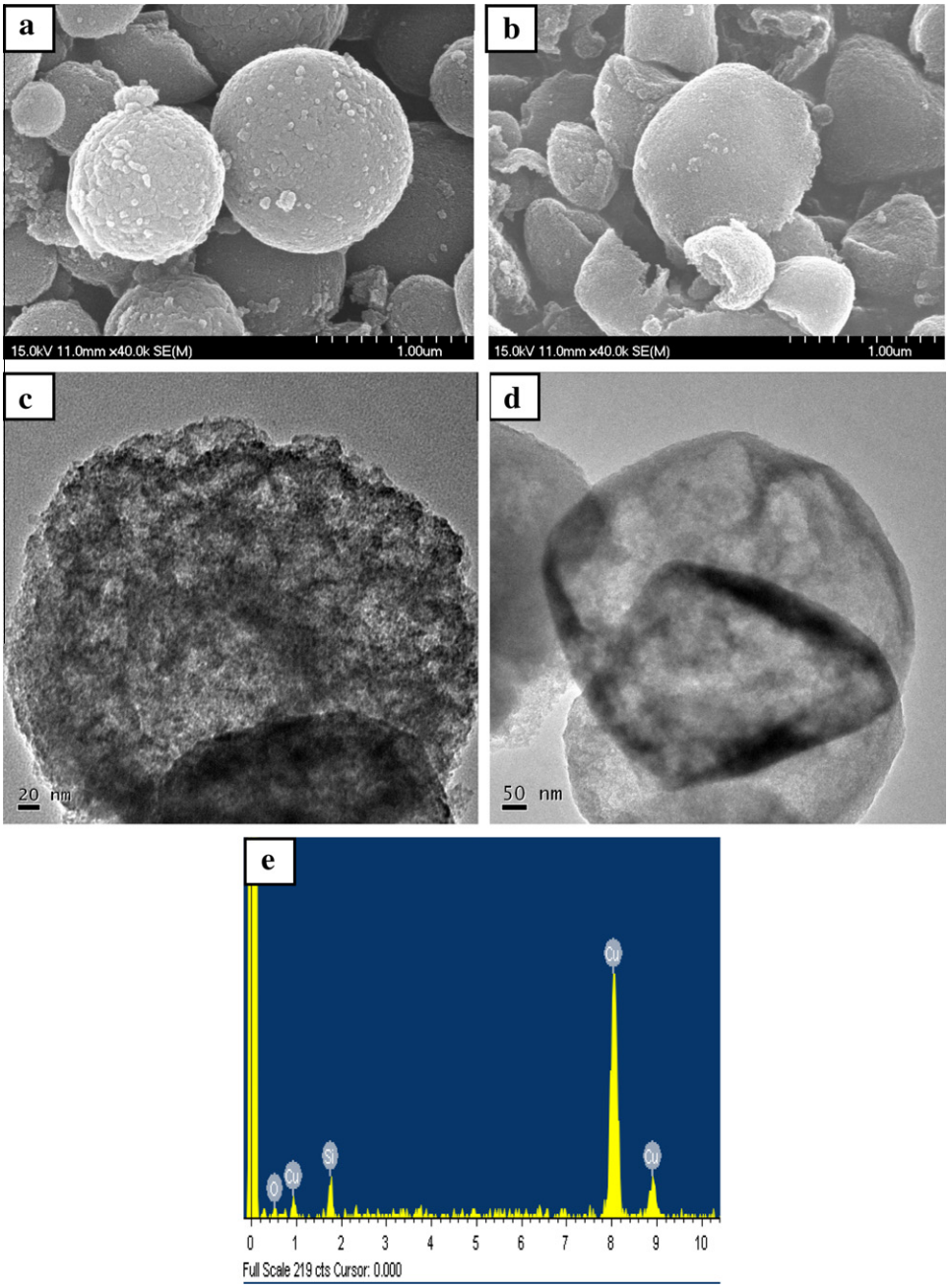


**Fig. 5.** SEM images of washed (a) MSPs($HNO_3$) and (b) MSPs(HCl); TEM images of washed (c) MSPs($HNO_3$) and (d) MSPs(HCl); (e) EDS spectrum of the washed MSPs($HNO_3$).

NaCl crystallites would be still in solid phase as solid shell because of its high melting point of 800 °C. Subsequently, the internal pressure would increase rapidly because the moisture cannot be released immediately, resulting in formation of crushed and hollow MSPs(HCl) particles.

### 3.2. $CO_2$ capture by TEPA-impregnated mesoporous silica-based adsorbents

Fig. 7 shows the time dependence of $CO_2$ uptake in the presence of 15% $CO_2$ at 60 °C for TEPA-impregnated MSPs($HNO_3$) and MSPs(HCl) adsorbents. In comparison, MCM-41, SBA-15, R-MCM-41 and R-SBA-15 materials synthesized from either pure silica chemical reagents or silicate supernatant extracted from TFT-LCD waste powder were also performed as supports of adsorbents for their adsorption performance and their physical characterization including XRD, $N_2$ physisorption measurement as well as TEM images were presented in Fig. S1, Fig. S2 and Fig. S3.It is seen that the $CO_2$ uptake increased rapidly to more than 90% of the maximum uptake within the first five minutes of adsorption before reaching a constant equilibrium value for all adsorbents. The $CO_2$ adsorption capacities of all adsorbents were in a range of 107–126 mg/g-adsorbent and follow the order of TEPA-MSPs(HCl) < TEPA-MCM-41 ≈ TEPA-R-MCM-41 < TEPA-SBA-15 < TEPA-MSPs($HNO_3$) < TEPA-R-SBA-15. This is probably due to that the textural properties of the mesoporous supports significantly influence the $CO_2$ adsorption performance.

In order to elucidate the effect of support structure on sorbent capacity, their textural properties were analyzed by $N_2$ physisorption technique with results shown in Fig. 8 and Table 2. It can be

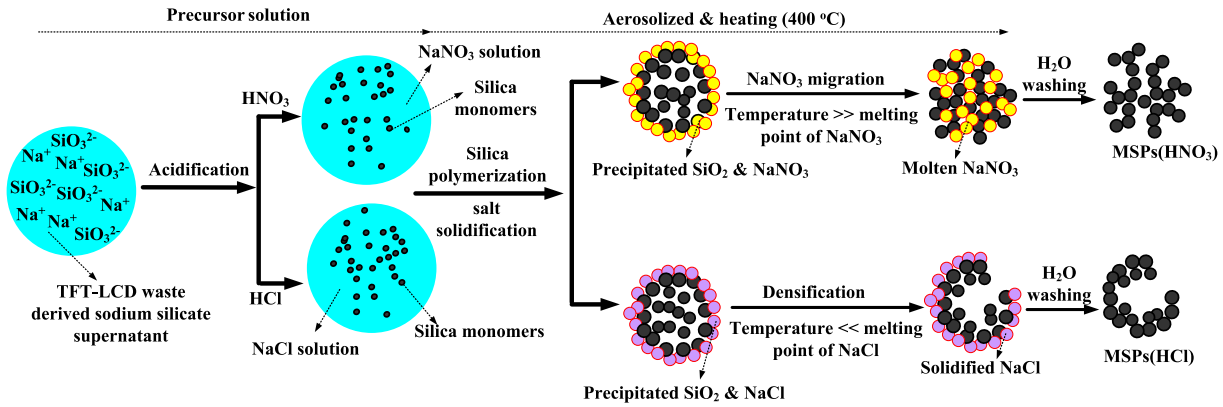


**Fig. 6.** Schematic representation showing the formation mechanism of MSPs(HCl) and MSPs($HNO_3$) samples through ultrasonic spray process.

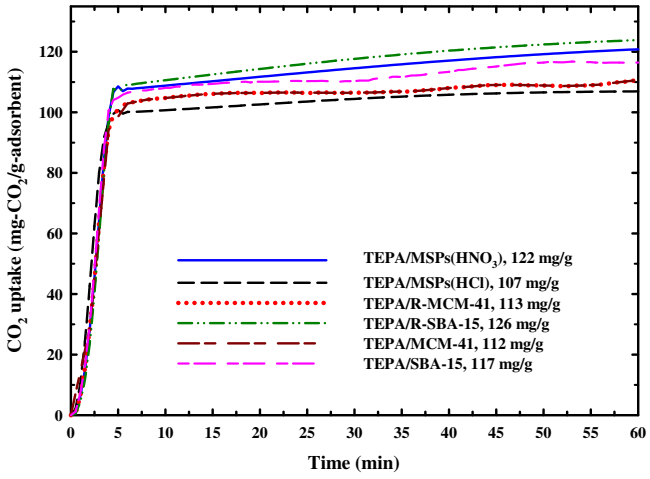


**Fig. 7.** $CO_2$ uptakes of TEPA-impregnated mesoporous silica supports of MSPs($HNO_3$), MSPs(HCl), R-MCM-41, R-SBA-15, MCM-41 and SBA-15.

seen from Fig. 8(a) that the adsorbents including MSPs(HCl) and R-MCM-41 exhibited type II isotherms of non-porous materials after TEPA impregnation, and this may suggest that their pores were nearly blocked. On the contrary, TEPA-SBA-15, TEPA-MSPs($HNO_3$) and TEPA-R-SBA-15 with larger pore volumes tended to maintain better meso-structures. BJH pore size distribution shown in Fig. 8(b) further reveals that parts of mesopores in SBA-15, MSPs($HNO_3$) and R-SBA-15 were still maintained after 50 wt.% TEPA impregnation, whereas the pores of MSPs(HCl) and R-MCM-41 were significantly diminished to be less than 2 nm after TEPA impregnation.

Since the density of TEPA is about 0.99 $cm^3/g$ and the total pore volumes of parent MSPs(HCl), MSPs($HNO_3$), R-MCM-41, SBA-15 and R-SBA-15 are 0.72 $cm^3/g$, 1.15 $cm^3/g$, 0.99 $cm^3/g$, 1.02 $cm^3/g$ and 1.50 $cm^3/g$, the maximum TEPA loading expected to load inside the channels of MSPs(HCl), MSPs($HNO_3$), R-MCM-41, SBA-15 and R-SBA-15 is 42%, 54%, 50%, 50.7% and 60%, respectively. Therefore, the pores of MSPs(HCl) and R-MCM-41were fully filled with 50 wt.% TEPA, and this may easily result in the blockage of effective adsorption sites and constricted pores, leading to decrease in adsorption capacity. On the other hand, it is noted that TEPA-R-SBA-15 exhibits superior adsorption capacity than that of TEPA-MSPs($HNO_3$) and TEPA-SBA-15. Because the pores of MSPs($HNO_3$), SBA-15 and R-SBA-15 were not completely filled by TEPA, there are enough accessible spaces in TEPA-MSPs($HNO_3$), TEPA-SBA-15 and TEPA-R-SBA-15 samples. Therefore, it could be speculated that the pore volume was not a main parameter which affected the sorbent capacity when the pores were not completely occupied. As seen from Fig. 8(b), compared with TEPA-SBA-15 and TEPA-MSPs($HNO_3$), TEPA-R-SBA-15 presents larger pore diameter and this could make the gas flow into TEPA-R-SBA-15 to be easier, which is beneficial for $CO_2$ adsorption. As a result, one may conclude that large pore diameter and large pore volume of the supports would combine together and result in high $CO_2$ capacity.

### 3.3. Comparison of mesoporous silica adsorbents for their $CO_2$ capture performance

TEPA-related mesoporous silica-based adsorbents for $CO_2$ capture from the literature and this work in terms of their starting precursors, manufacture process, structural properties, $CO_2$ adsorption performance as well as manufacturing cost are summarized in Table 3. It is observed that mesoporous R-MCM-41 and R-SBA-15 materials produced using TFT-LCD industrial waste silicates exhibit superior $CO_2$ adsorption performance and lower costs than those of MCM-41 and SBA-15 from pure silica chemicals; however, their industrial applications would be restricted due to the need of complex preparation procedures and long batch process times of several days.

The MSPs(TEOS) and MSPs(NaSi) produced by continuous aerosol method tend to have simple and faster production rates than mesoporous materials produced using batch reactors. Moreover, the use of spherical MSPs particles with higher packing density and higher volume-based adsorption capacity as supports of adsorbents can significantly reduce the adsorber volume of $CO_2$, and this has been another important issue that needs to be considered for field application [15,16]. But the prices for making MSPs(TEOS) and MSPs(NaSi) are still relatively high due to the use of expensive organic surfactants.

Avoiding the use of costly surfactants for the synthesis of mesoporous materials seems to be highly desirable and would be beneficial in terms of cost, environmental impact and scale-up potential. As seen from Table 3, unlike the mesoporous materials prepared via surfactant-templated routes, the surfactant-free synthesis of MSPs($HNO_3$) using silicate solution from TFT-LCD waste powder through continuous aerosol approach presents important advantages of fast synthesis, low manufacturing costs as well as superior $CO_2$ adsorption capacity. This will undoubtedly enhance the competitiveness for $CO_2$ capture in flue gas applications. Furthermore, this novel process could also be employed for further extensible to other kinds of Si-related industrial waste materials such as rice husk ash and coal flay ash, and it could be expected that the cost-effectiveness of the $CO_2$ capture technology and the

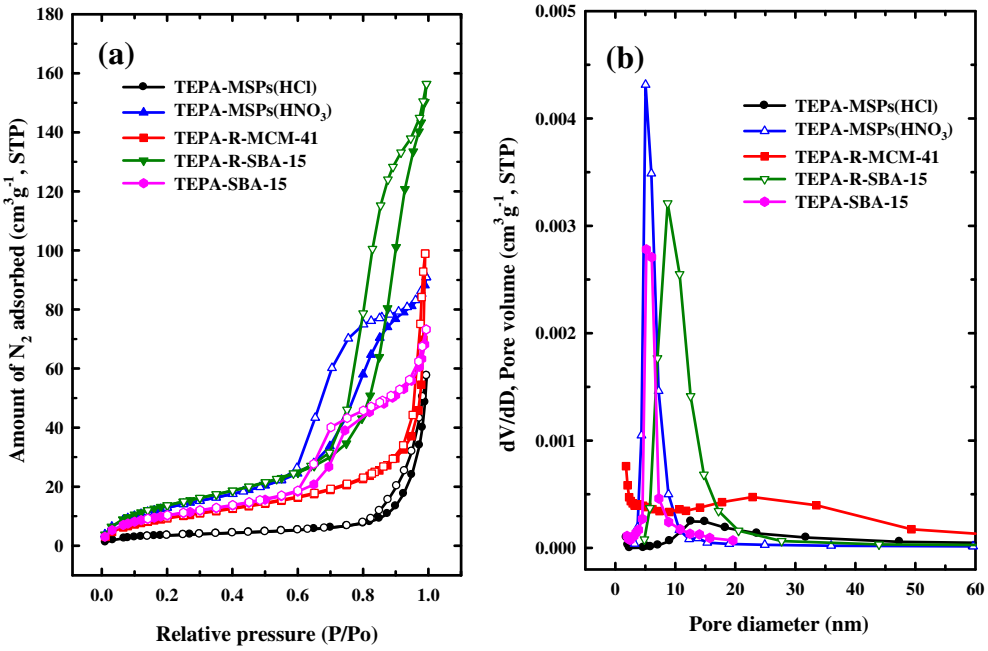


**Fig. 8.** (a) $N_2$ adsorption–desorption isotherms and (b) corresponding BJH pore size distributions of TEPA loaded on MSPs($HNO_3$), MSPs(HCl), R-MCM-41, R-SBA-15 and SBA-15 samples.

**Table 3**
Comparisons of TEPA-impregnated mesoporous silica-based adsorbents for $CO_2$ capture.

| Support | Precursor | Synthesis process | $S_{BET}$ ($m^2\ g^{-1}$) | $d_{BJH}$ (nm) | $V_p$ ($cm^3\ g^{-1}$) | Capacity (mg/g) | Relative price of chemicals | Reference |
|---|---|---|---|---|---|---|---|---|
| MSPs(TEOS) | TEOS + CTAB | Continuous process + calcination (4 h) calcination (4 h) | 1012 | 2.4 | 0.81 | 87 | – | [16] |
| MSPs(NaSi) | Sodium silicate + CTAB | Continuous process (4 s) + calcination (4 h) | 908 | 2.6 | 0.75 | 71 | 0.94 | [24] |
| MCM-41 | Sodium silicate + CTAB | Batch process (36 h) + calcination (4 h) | 1101 | 3.1 | 1.00 | 114 | 1.00[a] | This study |
| SBA-15 | Sodium silicate + P123 | Batch process (24 h) + tcalcination (6 h) | 745 | 6.5 | 1.02 | 117 | 0.41 | This study |
| R-MCM-41 | Waste powder + CTAB | Batch process (36 h) + calcination (4 h) | 1083 | 3.0 | 0.99 | 113 | 0.95 | This study |
| R-SBA-15 | Waste powder + P123 | Batch process (24 h) + calcination (6 h) | 661 | 9.1 | 1.50 | 126 | 0.24 | This study |
| MSPs($HNO_3$) | Waste powder | Continuous process (4 s) + washing | 776 | 5.3 | 1.15 | 122 | 0.02 | This study |

[a] The relative prices of chemicals were calculated based on the ratio of the purchase price of chemicals used for manufacturing the adsorbents to that for manufacturing the MCM-41.

waste treatment and disposal problem will be resolved simultaneously.

## 4. Conclusions

The present study presents a simple, cheap and well-suited for mass production approach to prepare mesoporous MSPs materials using silicate solution extracted from TFT-LCD industrial waste powder. The structural properties of the prepared MSPs materials can be easily controlled by altering the nature of the embedded salt templates. The XRD and $N_2$ physisorption analyses suggested that the obtained MSPs($HNO_3$) were pure siliceous materials with high specific surface area and large mesopores. Moreover, MSPs($HNO_3$) is considered as a better support of adsorbent in terms of $CO_2$ adsorption, which performs several advantages of simple and cost-effective synthesis as well as superior adsorption performance (122 mg-$CO_2$/g-adsorbent) than those of MCM-41 (112 mg-$CO_2$/g-adsorbent) and SBA-15 (117 mg-$CO_2$/g-adsorbent) materials. This novel route could be expected to be an alternative to the current methods for preparing potential and cost-effective materials for a wide range of applications.

## Acknowledgment

The authors gratefully acknowledge the financial support from the National Science Council of the Republic of China through Grant No. NSC 98-2221-E-009-023-MY3.

## Appendix A. Supplementary data

Supplementary data associated with this article can be found, in the online version, at http://dx.doi.org/10.1016/j.micromeso.2012.12.019.

## References


[1] J.D. Figueroa, T. Fout, S. Plasynski, H. McIlvried, R.D. Srivastava, Int. J. Green. Gas Control 2 (2008) 9–20.
[2] A.B. Rao, E.S. Rubin, Environ. Sci. Technol. 36 (2002) 4467–4475.
[3] X. Yan, L. Zhang, Y. Zhang, K. Qiao, Z. Yan, S. Komarneni, Chem. Eng. J. 168 (2011) 918–924.
[4] P.J.E. Harlick, A. Sayari, Ind. Eng. Chem. Res. 45 (2006) 3248–3255.
[5] S. Hao, H. Chang, Q. Xiao, Y. Zhong, W. Zhu, J. Phys. Chem. C 115 (2011) 12873–12882.
[6] X. Xu, C. Song, J.M. Andresen, B.G. Miller, A.W. Scaroni, Energy Fuels 16 (2002) 1463–1469.
[7] X. Yan, L. Zhang, Y. Zhang, G. Yang, Z. Yan, Ind. Eng. Chem. Res. 50 (2011) 3220–3226.
[8] C. Chen, W.-J. Son, K.-S. You, J.-W. Ahn, W.-S. Ahn, Chem. Eng. J. 161 (2010) 46–52.
[9] Y. Liu, J. Shi, J. Chen, Q. Ye, H. Pan, Z. Shao, Y. Shi, Micropor. Mesopor. Mater. 134 (2010) 16–21.
[10] M. Karthik, L.-Y. Lin, H. Bai, Micropor. Mesopor. Mater. 117 (2009) 153–160.
[11] S.H. Kim, B.Y.H. Liu, M.R. Zachariah, Langmuir 20 (2004) 2523–2526.
[12] N. Andersson, P.C. Alberius, J. Skov Pedersen, L. Bergström, Micropor. Mesopor. Mater. 72 (2004) 175–183.
[13] R. Pitchumani, J.J. Heiszwolf, A. Schmidt-Ott, M.-O. Coppens, Micropor. Mesopor. Mater. 120 (2009) 39–46.
[14] Y. Lu, H. Fan, A. Stump, T.L. Ward, T. Rieker, C.J. Brinker, Nature 398 (1999) 223–226.
[15] C. Lu, H. Bai, F. Su, W. Chen, J.F. Hwang, H.-H. Lee, J. Air Waste Manage. Assoc. 60 (2010) 489–496.
[16] H.C. Wang, C. Lu, H. Bai, J.F. Hwang, H.H. Lee, W. Chen, Y. Kang, S.-T. Chen, F. Su, S.-C. Kuo, F.-C. Hu, Appl. Surf. Sci. 258 (2012) 6943–6951.
[17] L.-Y. Lin, J.-T. Kuo, H. Bai, J. Hazard. Mater. 192 (2011) 255–262.
[18] X.S. Wu, F.Z. Wang, S. Nie, J.S. Liu, L. Yang, S.S. Jiang, Physica C: Supercon. 339 (2000) 129–136.
[19] H. Isobe, S. Utsumi, K. Yamamoto, H. Kanoh, K. Kaneko, Langmuir 21 (2005) 8042–8047.
[20] J. Schlomach, M. Kind, J. Colloid Interface Sci. 277 (2004) 316–326.
[21] Y. Liu, Y. Guo, Y. Zhu, D. An, W. Gao, Z. Wang, Y. Ma, Z. Wang, J. Hazard. Mater. 186 (2011) 1314–1319.
[22] T.-H. Liou, S.-J. Wu, J. Hazard. Mater. 171 (2009) 693–703.
[23] L. Zhang, W. Lu, R. Cui, S. Shen, Mater. Res. Bull. 45 (2010) 429–436.
[24] L.-Y. Lin, H. Bai, Micropor. Mesopor. Mater. 136 (2010) 25–32.